Activity-based proteomics of the endocannabinoid system

Rooden, E.J. van

Chapter 3

Chemical proteomics analysis of endocannabinoid hydrolase activity in Niemann-Pick Type C mouse brain[1]

Introduction

The endocannabinoid system (ECS) consists of the cannabinoid type 1 and 2 receptors (CB_1R and CB_2R) and their endogenous ligands: the endocannabinoids. The lipids anandamide (AEA) and 2-arachidonoylglycerol (2-AG) are the best characterized endocannabinoids.[2] The enzymes responsible for endocannabinoid biosynthesis and degradation are also part of the ECS, with most endocannabinoid degrading enzymes belonging to the serine hydrolase family (**Fig. 1**).[3] The combined activities of biosynthetic enzymes and degradative enzymes tightly regulate endocannabinoid concentrations in the brain. For example, 2-AG is mainly produced from 1-acyl-2-arachidonoylglycerol by the diacylglycerol lipases, DAGLα and DAGLβ, while it is degraded by monoacylglycerol lipase (MAGL) and to a minor extent by α,β-hydrolase domain-containing protein 6 (ABHD6) and α,β-hydrolase domain-containing protein 12 (ABHD12). Multiple pathways are known for the biosynthesis of anandamide, but they all use N-acylphosphatidylethanolamine (NAPE) as a central precursor, including the serine hydrolase ABHD4 and the β-metallolactamase N-acylphosphatidylethanolamine-phospholipase D (NAPE-PLD). NAPE is synthesized by the calcium-dependent N-acyltransferase PLA2G4E.[4] Fatty acid amide hydrolase (FAAH) terminates anandamide signaling by hydrolysis of its amide bond.

Endocannabinoid hydrolases that are part of the serine hydrolase superfamily can be studied using activity-based protein profiling (ABPP), a method which uses chemical probes for measuring enzyme activity in complex biological samples. Previously, ABPP was used to compare serine hydrolase activity in wildtype and CB_1R knockout mice.[5] Comparative ABPP has also been successfully applied in the identification of new drug targets.[6,7] With ABPP enzyme activities that are deregulated in a certain pathophysiological state can be identified and the relative amount of active enzyme copies as compared to wildtype situations can be quantified. The classical fluorophosphonate (FP)-based probes (FP-TAMRA and FP-biotin)[8] act as broad-spectrum serine hydrolase probes that label the endocannabinoid enzymes

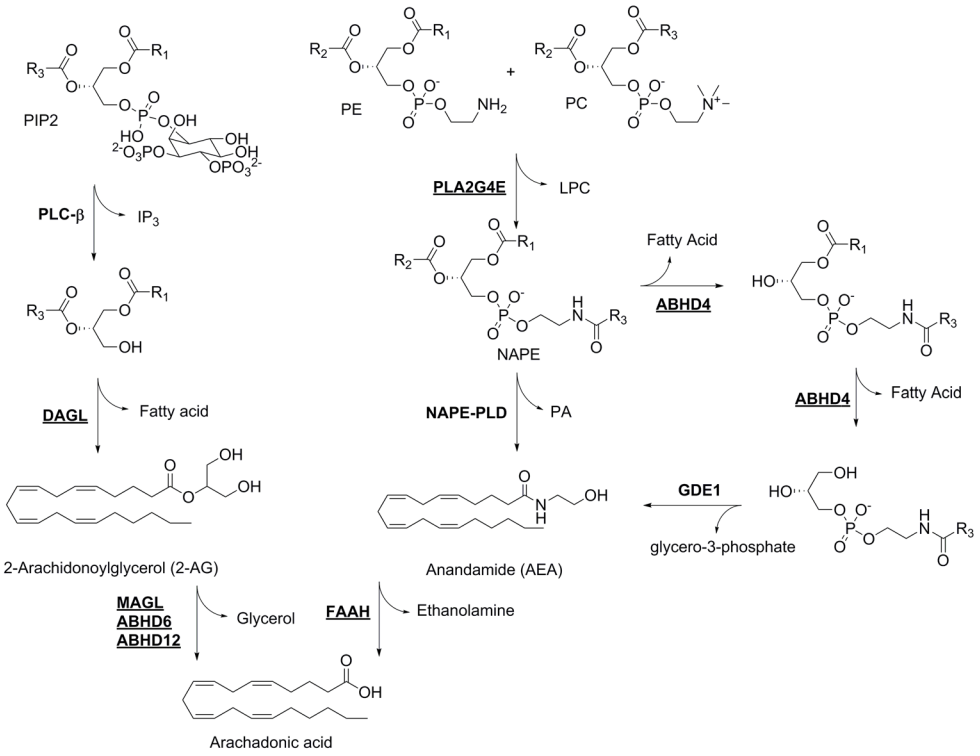

Figure 1 | Pathways for the biosynthesis and degradation of the endocannabinoids 2-AG and AEA. Enzymes with known activity-based probes are underlined. R_1/R_2: alkyl chains, R_3: arachidonoyl. ABHD; α/β-hydrolase domain-containing protein. AEA: anandamide. 2-AG: 2-arachidonoylglycerol. DAG: diacylglycerol. DAGL: diacylglycerol lipase. FAAH: fatty acid amide hydrolase. GDE1: glycerophosphodiesterase 1. LPC: lysophosphatidylcholine. MAGL: monoacylglycerol lipase. NAPE: N-acylphosphatidylethanolamine. PC: phosphatidylcholine. PE: phosphatidylethanolamine. PIP2: phosphatidylinositol 4,5-bisphosphate. PLA2G4E: phospholipase A2 group 4E. PLC: phospholipase C. PLD: phospholipase D.

FAAH, MAGL, PLA2G4E,[4] ABHD6 and ABHD4,[9,8] whereas the tailor-made tetrahydrolipstatin (THL)-based probes (MB064 and MB108) label both DAGL isoforms (alpha and beta) and ABHD4, ABHD6 and ABHD12.[5,10,11,12] Of note, the fluorescent probe DH379[11] targets DAGL and ABHD6.

Evaluation of endocannabinoid hydrolase activity in native tissue may provide insight in the role of the ECS in physiological and disease processes. Interestingly, endocannabinoid levels are elevated during neurodegeneration and neuroinflammation.[13,14,15] For example, endocannabinoid signaling is perturbed in various animal models of neurodegenerative diseases, including stroke,[16] traumatic brain injury,[17] Alzheimer's disease,[18] Huntington's disease,[19] Parkinson's disease[20,21] and multiple sclerosis.[22] It is hypothesized that regulation of ECS activity may provide therapeutic benefit for these type of neurological

diseases.[23]

Niemann-Pick Type C (NPC) is a neurodegenerative lysosomal storage disorder, which is associated with mutations in either of the genes encoding NPC1 or NPC2.[24] Both genes encode lysosomal proteins that are sequentially involved in cholesterol transport out of the lysosomes via a so far unknown mechanism. Defects in the function of the soluble NPC2 or the lysosomal membrane protein NPC1 leads to primary accumulation of cholesterol and secondary storage of sphingomyelin, sphingosine, and glycosphingolipids in lysosomes of multiple cell types, leading to visceral complications such as enlarged liver and spleen combined with progressive neurological disease.[23] There is no treatment available for Niemann-Pick type C patients. Additionally, there is no information available about the status of the ECS in Niemann-Pick. Therefore, endocannabinoid hydrolase activity was measured in the Niemann-Pick type C mouse model using ABPP.

Results

In 95% of the patients afflicted by Niemann-Pick type C, mutations in NPC1 are observed. Therefore, the role of the endocannabinoid system in this disease was investigated by comparison of endocannabinoid hydrolase activity between *Npc1*$^{+\backslash+}$ and *Npc1*$^{-\backslash-}$ mouse brains. First, labeling profiles of MB064, DH379 and FP-TAMRA in wildtype and knockout mouse brains was evaluated (**Fig. 2a**). Membrane and soluble fractions of both wildtype and knockout tissue were labeled with each probe separately, resolved on SDS-PAGE and visualized using in-gel fluorescence scanning. Coomassie staining was used as a protein loading control. The fluorescence intensity of the bands corresponding to DAGLα (~120 kDa), ABHD12 (~50 kDa), ABHD6 (~35 kDa) and FAAH (~60 kDa) were quantified to determine the relative enzyme activity between knockout and wildtype (**Fig. 2b**). Using the FP-TAMRA probe, the two bands corresponding to MAGL (~35 kDa) were observed, but due to band overlap with ABHD6 these cannot be accurately quantified. Labeling of DAGLα significantly decreased in the knockout mice as compared to wildtype, while ABHD6 and ABHD12 activity was the same. FAAH labeling was slightly decreased in the knockout, but this decrease was not statistically significant. In the cytosolic fraction, an increase in intensity of a 75 kDa-band as labeled by MB064 and FP-TAMRA was observed in the knockout brains. As reported previously,[5,29] DAGLα is identified as two separate bands, which can both be labeled with a DAGLα antibody and are absent in DAGLα KO mice (**Fig. 2d**). Remarkably, only the fluorescent band corresponding to the higher molecular weight was significantly decreased in the *Npc1*$^{-/-}$ mice as quantified by two separate probes MB064 and DH379 (**Fig. 2c**). To see if this observation was due to a decrease of protein abundance, a Western blot against DAGLα was performed (**Fig. 2e**). The signal of antibody labeling was quantified (**Fig. 2f**). The same pattern was observed for relative abundance as for relative

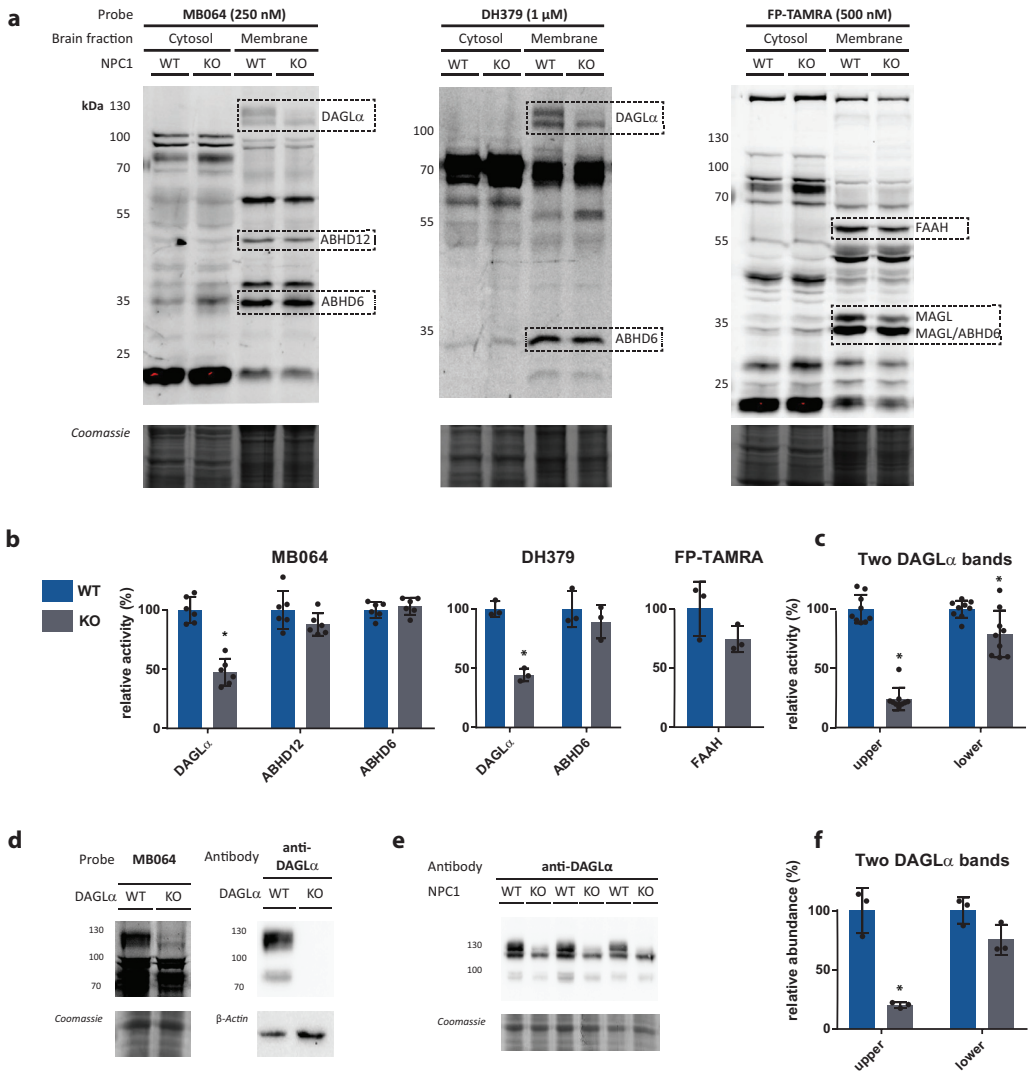

Figure 2 | Gel-based *Npc1*$^{+/+}$ (WT) vs *Npc1*$^{-/-}$ (KO) comparison. (**a**) Enzyme activity in the brain fractions as measured by the probes MB064, DH379 and FP-TAMRA. (**b**) Quantification of relative enzyme activity in WT and KO for probe targets (average WT is set to 100%). N = 3 (mice), n = 2 (MB064) or n = 1 (DH379 and FP-TAMRA). (**c**) Quantification of probe labeling of the two observed bands for DAGLα as measured by MB064 and DH379 (**Fig. 2a**). N = 3, n = 3. (**d**) DAGLα activity and abundance in DAGLα WT and KO mouse brain membrane proteome as measured by the probe MB064 and an anti-DAGLα antibody. (**e**) DAGLα abundance in NPC1 WT and KO mouse brain membrane proteome. (**f**) Quantification of antibody labeling of the two observed bands for DAGLα as measured by anti-DAGLα (blot **Fig. 2e**). Mean ± standard deviation is shown. * P < 0.05 (student's t-test).

activity: only the upper band corresponding to DAGLα is significantly decreased (**Fig. 2c**,**f**).

To study a broader range of serine hydrolases and to confirm the observations from the gel-based assay, a chemical proteomics method was employed using FP-biotin and MB108 to assess the role of the endocannabinoid system in NPC1. The enzymatic activity of 41 hydrolases in NPC1 knockout mouse brain were identified and compared with wildtype mouse brains (**Fig. 3**). In line with the gel-based ABPP, no significant difference in the endocannabinoid hydrolase activity was found (ABHD12, ABHD6, FAAH and MAGL) in NPC1 wildtype versus knockout mice brain proteomes. The activity of endocannabinoid hydrolase ABHD4 is also unaltered in knockout compared to wildtype. Remarkably, and in contrast to the gel-based ABPP results, DAGLα activity in knockout mice brain proteomes was not decreased compared to wildtype mice.

In a control experiment, biotinylated probe MB108 competes with both DAGLα bands labeled by the fluorescent probe MB064. Additionally, DAGL inhibitor DH376 did reduce DAGLα labeling in the chemical proteomics assay (**Fig. 4**). Finally, three hydrolases were significantly increased in knockout mouse brains compared to wildtype brains: retinoid-inducible serine carboxypeptidase (SCPEP1), cathepsin A (CTSA) and palmitoyl-protein thioesterase 1 (PPT1) (**Fig. 3**).

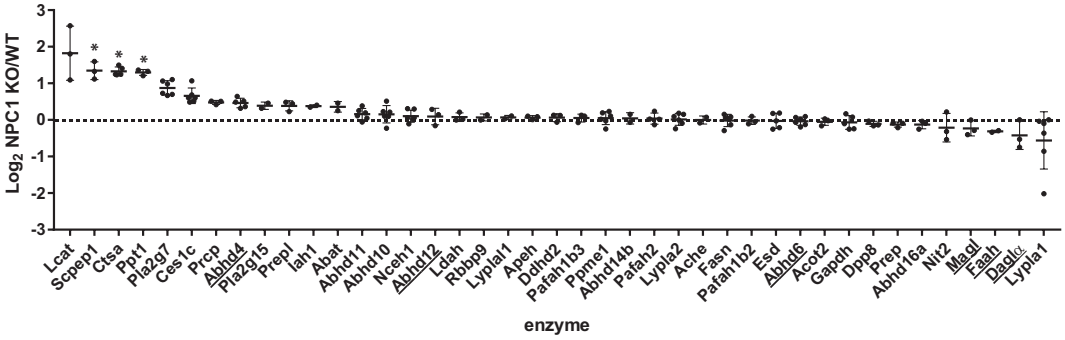

Figure 3 | Chemical proteomics comparison of *Npc1*$^{+/+}$ (WT) vs *Npc1*$^{-/-}$ (KO). Log_2 ratio of enzyme activity in KO brain proteome compared to WT. Activity was measured using FP-biotin or MB108 (both 10 µM, N = 3). The data from both probes was combined for both the cytosolic and membrane fraction. The mean and standard deviation is shown. Endocannabinoid related enzymes are underlined. Statistical analysis by means of student's t-test (each ratio was compared to a log_2 ratio of 0) and the resulting p-values were subjected to Benjamini-Hochberg correction, setting the false discovery rate at 10% (* indicates significant difference).

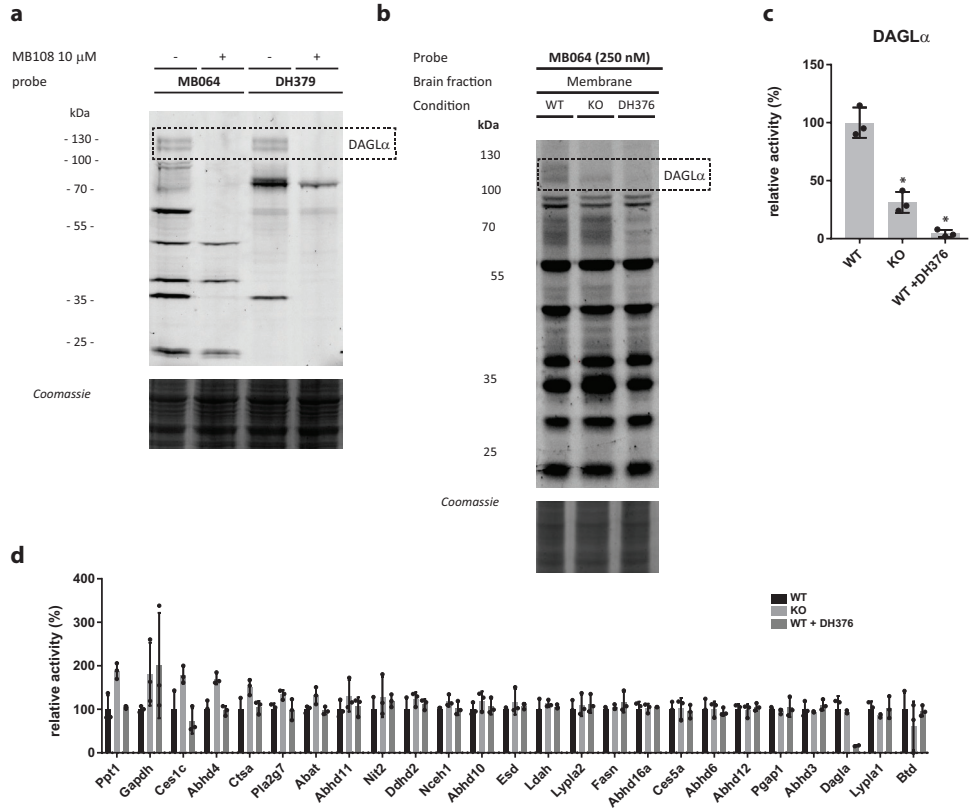

Figure 4 | Control experiments with MB108 and DAGLα inhibitor DH376 in mouse brain membrane proteome. (**a**) Gel-based *Npc1*$^{+/+}$ (WT) pre-treatment with MB108 and labeling with MB064 and DH379. (**b**) Gel-based *Npc1*$^{+/+}$ (WT) vs *Npc1*$^{-/-}$ (KO) comparison and competition with inhibitor DH376. (**c**) Quantification of relative enzyme activity for DAGLα (average WT is set to 100%), N = 3. * P < 0.05 (student's t-test). (**d**) Chemical proteomics comparison of *Npc1*$^{+/+}$ (WT) vs *Npc1*$^{-/-}$ (KO) and competition with DH376 (WT). Activity was measured in the membrane fraction using MB108 (10 µM). Label-free quantification with IsoQuant. Statistical analysis by means of student's t-test (KO and inhibitor conditions compared to WT) and the resulting p-values were subjected to Benjamini-Hochberg correction, setting the false discovery rate at 10% (* indicates significant difference).

Discussion

Niemann-Pick type C mice have previously been studied using activity-based protein profiling with a retaining β-glucosidase probe.[25] This study showed increased activity of the non-lysosomal glucosylceramidase (GBA2) in NPC1 knockout mice (and consistent increased abundance of the protein by Western blot). Importantly, pharmacological inhibition of GBA2 ameliorated the neuropathology of these mice.[25] Miglustat is approved as a drug, and initially thought to work through substrate reduction by inhibiting glucosylceramide synthase.[30] However, as was shown before, the molecular mechanism does not involve glucosylceramide synthase, and it is hypothesized that the therapeutic effect seems at least partly due to off-target inhibition of GBA2 by Miglustat.[25] It has been suggested that accumulation of sterols in lysosomes impaired in NPC1 (or NPC2) causes a more general lysosome dysfunction involving multiple hydrolases, such as lysosomal glucocerebrosidase (GBA).[31] Additionally, mutations in NPC1 or NPC2 genes result in severe progressive neurodegeneration. These observations led to the hypothesis that the hydrolases of the endocannabinoid system (ECS) might play a role in this disease.

Here, ABPP was used to quantify the activity of the endocannabinoid hydrolases FAAH, ABHD6, ABHD12, ABHD4 and MAGL in NPC1 knockout mice and it was found that their activity is not affected in wildtype vs NPC1 knockout mice. DAGLα activity seems to be decreased in the knockout mice based on the gel-based ABPP results. However, a discrepancy was found between the gel-based ABPP assay and the chemical proteomics assay in DAGLα activity between the NPC1 knockout mouse brains compared to wildtype mice. This discrepancy can possibly be caused by technical factors inherent to the two applied methodologies. In the gel-based ABPP assay only the labeling of the upper DAGLα-band was abolished in the NPC1 knockout brain proteome. It could be that the peptides from the protein corresponding to the upper band from the wildtype mouse proteome are not detected in the mass spectrometer due to post-translational modifications, such as phosphorylation, acetylation, methylation, palmitoylation or glycosylation. Peptides with such modifications are not found in this assay. If this would be true, a decrease in DAGLα activity in the NPC1 knockout mice would not be detected. Further experiments, such as direct quantification of 2-AG levels, are required to confirm a decrease in DAGLα activity in Niemann-Pick mice. In addition, it would be interesting to find the origin and role of the altered modification of DAGLα in Niemann-Pick type C. If the gel-based ABPP results are confirmed, it would be worthwhile to test the effects of a pharmacological intervention with DAGLα inhibitors, such as DH376 and DO34,[11] in Niemann-Pick disease models.

Finally, it was found that the activities of three non-endocannabinoid hydrolases, namely, CTSA, PPT1 and SCPEP1, were significantly elevated in NPC1 knockout mouse brains. These enzymes are lysosomal proteins, which is in line with the important role of NPC1 in lysosomes. SCPEP1 shows

homology with CTSA[32] and a study with double knockout of SCPEP1 and CTSA suggests they share the same peptide substrate.[33] Knockout of SCPEP1 in mice resulted in viable mice without lysosomal impairment.[32] Mutations in the CTSA gene cause galactosialidosis in humans[34] and secondary deficiencies of β-galactosidase and neuraminidase. This same phenotype is mirrored in a CTSA knockout mice mouse model.[35] The protective role of the enzyme for galactosidase and neuraminidase is a structural function of the enzyme: mice with catalytic serine-to-alanine mutation have normal levels of β-galactosidase and neuraminidase.[36] CTSA inhibitors have been tested in humans[37] and CTSA is a therapeutic target for the treatment of cardiovascular diseases.[38,39] Thus, it would be interesting to test CTSA inhibitors in Niemann-Pick models. Palmitoyl-protein thioesterase 1 (PPT1) is also a lysosomal enzyme[40] and the dysregulation of this enzyme causes a lysosomal storage and neurodegenerative disorder; infantile neuronal ceroid lipofuscinosis.[37] This enzyme removes palmitoyl modifications from proteins that are being degraded in the lysosome. In PPT1 knockout mice cholesterol catabolism is altered.[41] PPT1 has been proposed to hydrolyze 2-AG and might therefore be involved in the ECS.[42] *In vivo* active inhibitors for PPT1[43] have been identified and could therefore also be tested in Niemann-Pick models. To conclude, no altered activity was found of endocannabinoid hydrolases in a Niemann-Pick type C mouse model using a chemical proteomics assay. Three hydrolases were identified with upregulated activity in NPC1 knockout mice, which might be interesting therapeutic target for future studies.

Experimental

Animals. *Npc1*$^{-/-}$ mice, along with wildtype littermates (*Npc1*$^{+/+}$), were generated as published previously.[25] Briefly, the heterozygous BALB/c Nctr-Npc1^{m1N}/J mice (stock number 003092) were obtained from The Jackson Laboratory (Bar Harbor, USA). Mouse pups were genotyped according to published protocols.[26] The mice were housed at the Institute Animal Core Facility in a temperature- and humidity-controlled room with a 12 h light/dark cycle and given free access to food and water *ad libitum*. All animal protocols were approved by the Institutional Animal Welfare Committee of the Academic Medical Centre Amsterdam in the Netherlands. Animals were first anesthetized with a dose of Hypnorm (0.315 mg/mL fenyl citrate and 10 mg/mL fluanisone) and Dormicum (5 mg/mL midazolam) according to their weight. The given dose was 80 µL/10 g body weight. Blood was collected by a heart puncture followed by cervical dislocation. Brains were dissected, rinsed with phosphate-buffered saline (PBS), snap frozen in liquid N_2 and stored at -80°C for biochemistry. Brain tissue was obtained from six female mice, three wildtype and three knockout.

Preparation of mouse tissue proteome. The mouse brains were cut in half with a scalpel, separating the two hemispheres. The mouse brain halves were slowly thawed on ice. The thawed mouse brain halves were dounce homogenized in 1.5 mL cold (4 °C) lysis buffer (20 mM HEPES pH 7.2, 2 mM DTT, 1 mM $MgCl_2$, 25 U/mL benzonase) and incubated for 15 minutes on ice. The suspension was centrifuged (2500 *g*, 3 min, 4 °C) to remove debris. The supernatant was collected and transferred to an ultracentrifuge tube. The debris was resuspended in 0.25 mL lysis buffer and resubjected to centrifugation. The combined supernatants were collected and subjected to ultracentrifugation

(100,000 *g*, 45 min, 4 °C, Beckman Coulter, Type Ti70 rotor). This yielded the membrane fraction as a pellet and the cytosolic fraction in the supernatant. The supernatant was collected and the membrane fraction was suspended in 1.5 mL storage buffer (20 mM HEPES pH 7.2, 2 mM DTT). The total protein concentration was determined with Quick Start Bradford assay (Bio-Rad). Membranes and supernatant fractions were both diluted to either 1.0 mg/mL or 2.0 mg/mL (for proteomics and gel-based ABPP respectively) and were used directly or flash frozen in liquid nitrogen and stored in aliquots at -80 °C until use.

Gel-based ABPP. Mouse brain cytosol or membrane fraction (2.0 mg/mL) was incubated with activity-based probe MB064 (250 nM), TAMRA-FP (500 nM) or DH379 (1 µM) (20 min, rt, 2.5% DMSO). For the competition experiments with inhibitor DH376, this step was preceded by incubation with 100 nM inhibitor (30 min, rt, 2.5% DMSO). For the competition experiments with probe MB108, this step was preceded by incubation with 10 µM probe (30 min, 37 °C, 2.5% DMSO). Laemlli buffer was added to quench the protein activity and the mixture was allowed to stand at rt for at least five minutes before the samples were loaded and resolved on SDS-PAGE gel (10% acrylamide), together with PageRuler Plus Prestained Protein Ladder (Thermo Scientific). The gels were scanned using a ChemiDoc (Bio-Rad, Cy3 channel: expose 180 sec for MB064, 60 sec for DH379/TAMRA-FP, Cy5 channel 10 sec for marker). After fluorescent scanning, the gels were stained with a Coomassie staining solution (0.25% (w/v) Coomassie Brilliant Blue in 50% MeOH, 10% AcOH, 40% MilliQ (v/v/v)). The gels were scanned after destaining with MilliQ. Both the fluorescence and Coomassie images were analyzed using Image Lab 5.2. The Coomassie gel is used to determine protein loading (automatic lane/band detection, background subtraction not enabled, select whole lane as band). The fluorescence bands are quantified using automatic lane/band detection with background subtraction enabled. Using the Coomassie-corrected gel-fluorescence values the average is calculated for WT and KO and a two-sided student's t-test is performed. The activities of proteins were relatively quantified by setting the average WT at 100%.

Western Blot. After the SDS-PAGE gel was resolved and imaged, proteins were transferred to 0.2 µm polyvinylidene difluoride membranes with a Trans-Blot Turbo™ Transfer system (Bio-Rad). Membranes were washed with TBS (50 mM Tris, 150 mM NaCl) and blocked with 5% milk (w/v, Elk magere melkpoeder, FrieslandCampina) in TBST (50 mM Tris, 150 mM NaCl, 0.05% Tween 20) for 1 h at rt. Membranes were then incubated with the primary antibody anti-DAGLα (1:1000, Cell Signaling Technology, #13626) in 5% BSA (w/v) in TBST (o/n, 4˚C), washed with TBST, incubated with matching secondary antibody HRP-coupled-goat-anti-rabbit (1:5000, Santa Cruz, sc2030) in 5% milk in TBST (1 h, rt) and washed with TBST and TBS. Imaging solution (10 mL Luminol, 100 µL ECL enhancer, 3 µL H_2O_2) was added to develop membranes and chemiluminescence was detected on the ChemiDoc (Bio-Rad) using standard chemiluminescence settings. The signal was normalized to Coomassie staining and quantified with Image Lab 5.2.

Activity-based proteomics. Mouse brain membrane or soluble proteome (245 µL, 1.0 mg/mL) was incubated with 5 µL 0.5 mM MB108 (10 µM) or FP-Biotin (10 µM) for 1 h at rt. The labeling reaction was quenched and excess probe was removed by chloroform/methanol precipitation: 250 µL MilliQ, 666 µL MeOH, 166 µL $CHCl_3$, 150 µL MilliQ added subsequently to each sample with a brief vortex after each addition. After centrifugation (4000 rpm, 10 min) the top and bottom layer surrounding the floating protein pellet was removed. 600 µL MeOH was added and the pellet was resuspended by sonication with a probe sonicator (10 sec, 30% amplitude). After centrifugation (14,000 rpm, 5 min) the methanol was removed and the protein pellet was redissolved in 250 µL 6 M Urea/25 mM

ammonium bicarbonate and allowed to incubate for 15 minutes. 2.5 µL 1 M DTT was added and the mixture was heated to 65 °C for 15 minutes. The sample was allowed to cool to rt (~ 5 min) before 20 µL 0.5 M iodoacetamide was added and the sample was alkylated for 30 minutes in the dark. 70 µL 10% (wt/vol) SDS was added and the proteome was heated for 5 minutes at 65 °C. The sample was diluted with 2 mL PBS. 50 µL of 50% slurry of Avidin-Agarose from egg white (Sigma-Aldrich) was washed with PBS and added to the proteome sample in 1 mL PBS. The beads were incubated with the proteome for 3 h, while rotating. The beads were isolated by centrifugation (2500 *g*, 2 min) and washed with 0.5% (wt/vol) SDS in PBS (1x) and PBS (3x). The proteins were digested overnight with 500 ng sequencing grade trypsin (Promega) in 250 µL on-bead digestion buffer (100 mM Tris pH 8, 100 mM NaCl, 1 mM $CaCl_2$, 2% ACN) at 37 °C with vigorous shaking. The pH was adjusted with formic acid to pH 3 and the beads were removed. The peptides were isotopically labeled by on-stage tip dimethyl labeling. Wildtype and knockout samples were differently labeled with isotopic dimethyl labeling and combined after labeling to allow comparison (wildtype light and knockout heavy). The stage tips were made by inserting C18 material in a 200 µL pipet tip. The stepwise procedure given in the table below was followed for stage tip desalting and dimethyl labeling. The solutions were eluted by centrifugal force and the constitutions of the reagents are given below. For label-free quantification samples, step 6 and 7 are omitted.

Step	Aim	Solution	Centrifugation
1	Conditioning	Methanol (50 µL)	2 min 600 *g*
2	Conditioning	Stage tip solution B (50 µL)	2 min 600 *g*
3	Conditioning	Stage tip solution A (50 µL)	2 min 600 *g*
4	Loading	Load samples on stage tips	2.5 min 800 *g*
5	Washing	Stage tip solution A (100 µL)	2.5 min 800 *g*
6	Dimethyl labeling (5x)	20/20/40/40/30 µL L or M reagent	5 min 400 *g*
7	Washing	Stage tip solution A (100 µL)	2.5 min 800 *g*
8	Elution	Stage tip solution B (100 µL)	2.5 min 800 *g*

Stage tip solution A is 0.5% (vol/vol) FA in H_2O. Stage tip solution B is 0.5% (vol/vol) FA in 80% (vol/vol) ACN in H_2O. Dimethyl labeling reagents: Phosphate buffer (50 mM; pH 7.5) with $NaBH_3CN$ 0.03 M containing either 2% (vol/vol) CH_2O (Light) or CD_2O (Medium). After the final elution step, the desired heavy and light samples were combined and concentrated on a Speedvac to remove the ACN. The residue was reconstituted in 95/3/0.1 H_2O/ACN/FA (vol/vol) before LC/MS analysis. Labelled peptides were measured on an Orbitrap. Label-free peptides were measured on a Synapt mass spectrometer.

Orbitrap. Tryptic peptides were analyzed on a Surveyor nanoLC system (Thermo) hyphenated to a LTQ-Orbitrap mass spectrometer (Thermo) as previously described. Briefly, emitter, trap and analytical column (C18, 120 Å) were purchased from Nanoseparations (Nieuwkoop, The Netherlands) and mobile phases (A: 0.1% formic acid/H_2O, B: 0.1% formic acid/ACN) were made with ULC/MS grade solvents (Biosolve). General mass spectrometric conditions were: electrospray voltage of 1.8-2.5 kV, no sheath and auxiliary gas flow, capillary voltage 40 V, tube lens voltage 155 V and ion transfer tube temperature 150 °C. Polydimethylcyclosiloxane (m/z = 445.12002) and dioctyl phthalate ions (m/z = 391.28429) from the environment were used as lock mass. Some 10 µL of the samples was pressure loaded on the trap column for 5 min with a 10 µL/min flow and separated with a gradient of 35 min

5%–30% B, 15 min 30%–60% B, 5 min A at a flow of 300 µL/min split to 250 nL/min by the LTQ divert valve. Full MS scans (300–2000 m/z) acquired at high mass resolution (60,000 at 400 m/z, maximum injection time 1000 ms, AGC 106) in the Orbitrap was followed by three MS/MS fragmentations in the LTQ linear ion trap (AGC 5x103, max inj time 120 ms) from the three most abundant ions. MS/MS settings were: collision gas pressure 1.3 mT, normalized collision energy 35%, ion selection threshold of 750 counts, activation q = 0.25 and activation time 30 ms. Ions of z < 2 or unassigned were not analyzed and fragmented precursor ions were measured twice within 10 s and were dynamically excluded for 60 s. Data analysis was performed using Maxquant with acetylation (protein N term) and oxidation (M) as variable modifications. The false discovery rate was set at 1% and the peptides were screened against reviewed mouse proteome (Uniprot). Serine hydrolases that were identified in at least two repetitive experiments and for which at least one unique peptide and two peptides in total were identified were considered as valid quantifiable hits. For proteins identified by both probes, the normalized ratios from Maxquant were combined for further analysis. The binary logarithm of each ratio was compared to 0 with a student's t-test. The resulting p-values were subjected to a Benjamini-Hochberg correction, setting the false discovery rate at 10% (q=0.1). Briefly, the p-values of all quantifiable hits were ordered from lowest to highest, and the Benjamini-Hochberg statistic was calculated as q * (position in the list) divided by the number of tests. Subsequently, the proteins for which the p-value is smaller than the BH statistic are controlled for a FDR of q*10%.

Synapt. The peptides were measured as described previously for the NanoACQUITY UPLC System coupled to SYNAPT G2-Si high definition mass spectrometer. A trap-elute protocol, where 1 µL of the digest is loaded on a trap column (C18 100 Å, 5 µM, 180 µM x 20 mm, Waters) followed by elution and separation on the analytical column (HSS-T3 C18 1.8 µM, 75 µM x 250 mm, Waters). The sample is brought onto this column at a flow rate of 10 µL/min with 99.5% solvent A for 2 min before switching to the analytical column. Peptide separation is achieved using a multistep concave gradient based on the gradients used in Distler et al.[27] The column is re-equilibrated to initial conditions after washing with 90% solvent B. The rear seals of the pump are flushed every 30 min with 10% (vol/vol) ACN. [Glu^1]-fibrinopeptide B (GluFib) is used as a lock mass compound. The auxiliary pump of the LC system is used to deliver this peptide to the reference sprayer (0.2 µL/min). A UDMS^e method is set up as described in Distler *et al*.[27] Briefly, the mass range is set from 50 to 2,000 Da with a scan time of 0.6 seconds in positive, resolution mode. The collision energy is set to 4 V in the trap cell for low-energy MS mode. For the elevated energy scan, the transfer cell collision energy is ramped using drift-time specific collision energies.[28] The lock mass is sampled every 30 seconds. Raw data is processed in PLGS (v3.0.3) and ISOQuant v1.5.

Data availability. The mass spectrometry proteomics datasets generated for this study have been deposited to the ProteomeXchange Consortium via the PRIDE[44] partner repository with the dataset identifier PXD008979.

References

1. Eva J. van Rooden, Annelot C. M van Esbroeck, Marc P. Baggelaar, Hui Deng, Bogdan I. Florea, André R. A. Marques, Roelof Ottenhoff, Rolf G. Boot, Herman S. Overkleeft, Johannes M. F. G. Aerts, Mario van der Stelt. Chemical proteomics analysis of endocannabinoid hydrolase activity in Niemann-Pick Type C mouse brain. *Frontiers in Neuroscience*, **2018**, 12:440.
2. Marzo, V. Di, Bifulco, M. & Petrocellis, L. De. The endocannabinoid system and its therapeutic exploitation. *Nat. Rev. Drug Discov.* **3**, 771–784 (2004).
3. Blankman, J. L. & Cravatt, B. F. Chemical probes of endocannabinoid metabolism. *Pharmacol. Rev.* **65**, 849–71 (2013).
4. Ogura, Y., Parsons, W. H., Kamat, S. S. & Cravatt, B. F. A calcium-dependent acyltransferase that produces N-acyl phosphatidylethanolamines. *Nat. Chem. Biol.* **12**, 1–5 (2016).
5. Baggelaar, M. P. *et al.* Chemical Proteomics Maps Brain Region Specific Activity of Endocannabinoid Hydrolases. *ACS Chem. Biol.* **12**, 852–861 (2017).
6. Nomura, D. K., Dix, M. M. & Cravatt, B. F. Activity-based protein profiling for biochemical pathway discovery in cancer. *Nat. Rev. Cancer* **10**, 630–638 (2010).
7. Nomura, D. K. *et al.* Monoacylglycerol Lipase Regulates a Fatty Acid Network that Promotes Cancer Pathogenesis. *Cell* **140**, 49–61 (2010).
8. Liu, Y., Patricelli, M. P. & Cravatt, B. F. Activity-based protein profiling: The serine hydrolases. *Proc. Natl. Acad. Sci.* **96**, 14694–14699 (1999).
9. Simon, G. M. & Cravatt, B. F. Activity-based proteomics of enzyme superfamilies: Serine hydrolases as a case study. *J. Biol. Chem.* **285**, 11051–11055 (2010).
10. Baggelaar, M. P. *et al.* Development of an activity-based probe and in silico design reveal highly selective inhibitors for diacylglycerol lipase-α in brain. *Angew. Chem. Int. Ed.* **52**, 12081–12085 (2013).
11. Ogasawara, D. *et al.* Rapid and profound rewiring of brain lipid signaling networks by acute diacylglycerol lipase inhibition. *Proc. Natl. Acad. Sci.* **113**, 26–33 (2016).
12. Baggelaar, M. P. *et al.* A highly selective, reversible inhibitor identified by comparative chemoproteomics modulates diacylglycerol lipase activity in neurons. *J. Am. Chem. Soc.* **137**, 8851–8857 (2015).
13. Nomura, D. K. *et al.* Endocannabinoid Hydrolysis Generates Brain Prostaglandins That Promote Neuroinflammation. *Science.* **334**, 809–814 (2011).
14. van der Stelt, M. & Di Marzo, V. Cannabinoid Receptors and Their Role in Neuroprotection. *NeuroMolecular Med.* **7**, 37–50 (2005).
15. Chiurchiù, V., van der Stelt, M., Centonze, D. & Maccarrone, M. The endocannabinoid system and its therapeutic exploitation in multiple sclerosis: Clues for other neuroinflammatory diseases. *Prog. Neurobiol.* **160**, 82–100 (2017).
16. Hillard, C. Role of Cannabinoids and Endocannabinoids in Cerebral Ischemia. *Curr. Pharm. Des.* **14**, 2347–2361 (2008).
17. Schurman, L. D. & Lichtman, A. H. Endocannabinoids: A promising impact for traumatic brain injury. *Front. Pharmacol.* **8**, 1–17 (2017).
18. Bisogno, T. & Di Marzo, V. The role of the endocannabinoid system in Alzheimer's disease: facts and hypotheses. *Curr. Pharm. Des.* **14**, 2299–3305 (2008).
19. Maccarrone, M., Battista, N. & Centonze, D. The endocannabinoid pathway in Huntington's disease: A comparison with other neurodegenerative diseases. *Prog. Neurobiol.* **81**, 349–379 (2007).
20. Di Marzo, V., Hill, M. P., Bisogno, T., Crossman, A. R. & Brotchie, J. M. Enhanced levels of endogenous cannabinoids in the globus pallidus are associated with a reduction in movement in an animal model of Parkinson's disease. *FASEB J.* **14**, 1432–1438 (2000).

21. Maccarrone, M. *et al.* Levodopa treatment reverses endocannabinoid system abnormalities in experimental parkinsonism. *J. Neurochem.* **85**, 1018–1025 (2003).
22. Baker, D. *et al.* Endocannabinoids control spasticity in a multiple sclerosis model. *FASEB J.* **15**, 300–302 (2000).
23. Scotter, E. L., Abood, M. E. & Glass, M. The endocannabinoid system as a target for the treatment of neurodegenerative disease. *Br. J. Pharmacol.* **160**, 480–498 (2010).
24. Vanier, M. & Millat, G. Niemann-Pick disease type C. *Clin. Genet.* **64**, 269–281 (2003).
25. Marques, A. R. a *et al.* Reducing GBA2 Activity Ameliorates Neuropathology in Niemann-PickType C Mice. *PLoS One* **10**, 1–18 (2015).
26. Loftus, S. K. *et al.* Murine Model of Niemann-Pick C Disease: Mutation in a Cholesterol Homeostasis Gene. *Science.* **277**, 232–236 (1997).
27. Distler, U., Kuharev, J., Navarro, P. & Tenzer, S. Label-free quantification in ion mobility–enhanced data-independent acquisition proteomics. *Nat. Protoc.* **11**, 795–812 (2016).
28. Distler, U. *et al.* Drift time-specific collision energies enable deep-coverage data-independent acquisition proteomics. *Nat. Methods* **11**, 167–70 (2014).
29. Gao, Y. *et al.* Loss of Retrograde Endocannabinoid Signaling and Reduced Adult Neurogenesis in Diacylglycerol Lipase Knock-out Mice. *J. Neurosci.* **30**, 2017–2024 (2010).
30. Nietupski, J. B. *et al.* Iminosugar-based inhibitors of glucosylceramide synthase prolong survival but paradoxically increase brain glucosylceramide levels in Niemann-Pick C mice. *Mol. Genet. Metab.* **105**, 621–628 (2012).
31. Ferraz, M. J. *et al.* Lyso-glycosphingolipid abnormalities in different murine models of lysosomal storage disorders. *Mol. Genet. Metab.* **117**, 186–193 (2016).
32. Kollmann, K. *et al.* Molecular characterization and gene disruption of mouse lysosomal putative serine carboxypeptidase 1. *FEBS J.* **276**, 1356–1369 (2009).
33. Pan, X. *et al.* Serine Carboxypeptidase SCPEP1 and Cathepsin A Play Complementary Roles in Regulation of Vasoconstriction via Inactivation of Endothelin-1. *PLoS Genet.* **10**, (2014).
34. Galjart, N. J., Gillemans, N., Meijer, D. & D'Azzo, A. Mouse 'Protective Protein'. *J. Biol. Chem.* **265**, 4678–4684 (1990).
35. Korah, N., Smith, C. E., D'Azzo, A., Mui, J. & Hermo, L. Characterization of Cell- and Region-Specific Abnormalities in the Epididymis of Cathepsin A Deficient Mice. *Mol. Reprod. Dev.* **66**, 358–373 (2003).
36. Seyrantepe, V. *et al.* Enzymatic activity of lysosomal carboxypeptidase (cathepsin) a is required for proper elastic fiber formation and inactivation of endothelin-1. *Circulation* **117**, 1973–1981 (2008).
37. Tillner, J. *et al.* Tolerability, safety, and pharmacokinetics of the novel cathepsin A inhibitor SAR164653 in healthy subjects. *Clin. Pharmacol. Drug Dev.* **5**, 57–68 (2016).
38. Schreuder, H. A. *et al.* Crystal structure of cathepsin A, a novel target for the treatment of cardiovascular diseases. *Biochem. Biophys. Res. Commun.* **445**, 451–456 (2014).
39. Petrera, A. *et al.* Cathepsin A inhibition attenuates myocardial infarction-induced heart failure on the functional and proteomic levels. *J. Transl. Med.* **14**, 153 (2016).
40. Lu, J. Y., Verkruyse, L. A. & Hofmann, S. L. The effects of lysosomotropic agents on normal and INCL cells provide further evidence for the lysosomal nature of palmitoyl-protein thioesterase function. *Biochim. Biophys. Acta - Mol. Cell Biol. Lipids* **1583**, 35–44 (2002).
41. Ahtiainen, L. *et al.* Palmitoyl protein thioesterase 1 (Ppt1)-deficient mouse neurons show alterations in cholesterol metabolism and calcium homeostasis prior to synaptic dysfunction. *Neurobiol. Dis.* **28**, 52–64 (2007).
42. Wang, R. *et al.* Identification of palmitoyl protein thioesterase 1 in human thp1 monocytes and macrophages and characterization of unique biochemical activities for this enzyme. *Biochemistry* **52**, 7559–7574 (2013).

43. Cognetta, A. B. *et al.* Selective N-Hydroxyhydantoin Carbamate Inhibitors of Mammalian Serine Hydrolases. *Chem. Biol.* **22**, 928–937 (2015).
44. Vizcaíno, J. A. *et al.* 2016 update of the PRIDE database and its related tools. *Nucleic Acids Res.* **44**, D447–D456 (2016).